Turkish Journal of Electrical Engineering & Computer Sciences

http://journals.tubitak.gov.tr/elektrik/

Research Article

Turk J Elec Eng & Comp Sci
(2016) 24: 1446 – 1460

doi:10.3906/elk-1310-61

A simple hybrid method for segmenting vessel structures in retinal fundus images

Cemal KÖSE*
Department of Computer Engineering, Faculty of Engineering, Karadeniz Technical University, Trabzon, Turkey

Received: 07.10.2013 • **Accepted/Published Online:** 31.03.2014 • **Final Version:** 23.03.2016

Abstract: In this paper, a simple, fast, and efficient hybrid segmentation method is presented for extracting vessel structures in retinal fundus images. Basically, this hybrid approach combines circular and naive Bayes classifiers to extract blood vessels in retinal fundus images. The circular method samples pixels along the enlarging circles centered at the current pixel and classifies the current pixel as vessel or nonvessel. An elimination technique is then employed to eliminate the nonvessel fragments from the processed image. The naive Bayes method as a supervised technique uses a very small set of features to segment retinal vessels in retinal images. The designed hybrid method exploits the circular and Bayesian segmentation results together to achieve the best performance. The achieved performance of the segmentation methods are tested on DRIVE and STARE databases for evaluation. The proposed methods segment a retinal image within 1 s and achieve about 95% accuracy. The results also indicate that the proposed hybrid method is one of the simplest and efficient segmentation methods among the unsupervised and supervised methods in the literature.

Key words: Medical image processing, retinal vessel segmentation, circular segmentation, Bayesian segmentation, hybrid segmentation, automatic segmentation

1. Introduction

Automatic segmentation and measurement of vessel structures are main research areas in retinal image analysis, which are extremely important in detecting and monitoring eye illnesses and taking early precautions for their effective treatment. Automatic systems are required to perform labor and computationally intensive tasks including extraction, measurement, visualization, and evaluation of retinal blood vessels. A standard grading system is used in manual assessment of retinal images. Manual assessment also requires ophthalmologists or professionally trained graders to analyze large numbers of retinal fundus images. In manual evaluation, segmentation and measurement accuracy also varies depending on the quality of the retinal images and graders' ability and experience. Furthermore, manual segmentation and measurement processes can take up to 1 h for evaluation of only a single eye. Thus, a fully automated computer system extracting and measuring the vessel structures in retinal images could definitely reduce the workload of eye clinicians.

Visual properties of retinal blood vessels are exploited in the diagnosis of many retinal diseases such as glaucoma, arteriosclerosis, hypertension, and diabetic retinopathy. To give an example, retinal blood vessels are used as landmarks for locating the optic disk, macula, and lesions [1]. In order to monitor the progress of a retinal disease such as diabetic retinopathy, the retinal fundus images are taken and analyzed periodically (e.g., every 6 or more months). Early detection of retinal diseases based on changes in blood vessels may prevent

*Correspondence: ckose@ktu.edu.tr

visual loss [2]. Hence, to reduce the burden on medical professionals, changes in blood vessels are automatically analyzed to create an opportunity for early diagnosis of retinal diseases.

Retinal vessels also have many observable characteristics, including opacity or reflectivity, tortuosity or relative curvature, normal or abnormal branching, color, and size. Measurements of these characteristics are important for diagnosis and treatment of many retinal diseases as well as clinical research studies [3–6]. The structure and position of retinal vessels can also be exploited in monitoring retinal diseases such as age-related macular degeneration and diabetic retinopathy. They are also used in finding the location of the optic disk and fovea, and in reducing the number of false positives in detection of microaneurysms [7,8].

In general, automatic evaluation of blood vessel anomalies in retinal fundus images requires segmentation of vessels. Even though many methods have been proposed for vessel segmentation in previous studies, there is still room for improvement of existing methods in the area. In addition, the employed segmentation algorithm has to be fast. The proposed method should also not be completely dependent on some configuration parameters. Therefore, the motivation in this study is to develop a simple, efficient, fast, and easily usable vessel segmentation method that only depends on a few tunable threshold values.

As indicated above, existing methods need to be improved in terms of at least one of the following drawbacks. First, lack of adaptive capabilities under varying image conditions may result in poor quality of segmentation, such as under- and oversegmentation. Second, for extracting vessel structures in the retinal images, the methods involve complex preprocessing and postprocessing operations, which results in increased computational cost. Third, user involvement is needed to select the region of interest, which shows that the methods are not completely automatic. Finally, segmentation and evaluation processes themselves require too much computational effort. In this paper, three simple, fast, and quite efficient approaches are introduced for segmenting retinal vessels. These are circular, Bayesian, and hybrid segmentations approaches. The circular segmentations method with a few easily adjustable thresholds is algorithmically and computationally quite simple. The Bayesian method with selective sampling can easily be trained for efficient segmentation. The hybrid segmentation method combines circular and naive Bayes approaches for the best performance.

The rest of this paper is organized as follows. A summary of other segmentation approaches is given in Section 2. Implementation details of the proposed system with employed basic techniques and the segmentation techniques of the circular, Bayesian, and hybrid approaches are given in Section 3. Measurement and evaluation methods are presented in Section 4. The results are discussed in Section 5. Finally, the conclusions and future works are presented in Section 6.

1.1. Previous approaches for segmenting blood vessels in retinal fundus images

Many retinal vessel segmentation techniques are employed to extract vessel structures in retinal fundus images [9–11]. These techniques may be classified as model-based, tracking, propagation, neural network, pattern recognition, and intelligent techniques [12–16]. Another classification approach groups the methods as window-based (unsupervised methods), classification-based (supervised methods), and tracking-based (unsupervised methods), as described in [17]. Therefore, the existing segmentation methods can be classified as supervised and unsupervised methods that are also called rule-based methods [18,19]. Another algorithm employs the cellular neural network models for classifying the pixels in the retinal images.

The rule-based and vessel tracking algorithms include the matched filter response and model-based locally adaptive thresholding methods, adaptive snake, and morphological methods. Tracking methods use a model to incrementally proceed along the vessels. Many different vessel tracking approaches are used to obtain and

evaluate vessel structures, vessel diameters, and branching points. These approaches include vessel tracking, adaptive or deformable models, and morphology-based techniques [20–22]. The matched filter response and piecewise threshold probing methods are employed for segmenting retinal vessels. Setting the rules for different vessels' structures is also difficult, which increases the computational complexity.

Another group of algorithms including supervised methods need labeled images for training. In the application of supervised methods, the segmentation criteria are obtained from the ground truth data based on known features. Therefore, labeling a single retinal image may take up to 1 or 2 h of processing. Features such as width of the vessels, edge strength, and intensity were used for segmentation by Staal et al. [23]. In another study, the Gabor wavelet transform was employed for segmentation by Soares et al. [24]. A supervised method using gray level and moment invariants-based features was introduced by Marin et al. [25] and a semisupervised method based on the radial projection was proposed by You et al. [26]. Performance of the supervised methods exploiting the preclassified data is usually better than that of unsupervised methods, and they usually generate very good segmentation results for retinal images without degenerations.

In the application, an unsupervised method evaluates and assigns pixels to a vessel according to some predefined criteria. An adaptive local thresholding method for retinal vessel segmentation was proposed in [27]. Another method for extracting vessels in pathological retinal images was suggested in [28]. This method extracts the vessel-like structures by employing the Laplacian operator.

The matched filters were used in detection of vessels in retinal images. The method first calculates the matched filter response image from the original retinal image [29]. Setting the matched filter for all vessel structures is difficult and increases computational complexity. The 2-D Gabor wavelet and supervised classification methods use a feature vector with different scales obtained from Gabor wavelet transform for each pixel. The features are exploited in the classification of each pixel as either vessel or nonvessel. A Bayesian method using class-conditional probability density functions is exploited in the classification. Some of the drawbacks of the method are the computational needs in the training phase, the need for manual labeling of the training data, and the lack of adaptation ability of the method for different data. The ridge-based vessel segmentation method, using image primitives to compute a probability of a line element as the feature of vessels, exploits the essential properties such as elongated structures of the vessels. One of the major disadvantages of the method is the need for manual labeling of the training data.

In this study, a simple and fast method is given for segmenting vessels, which produces a full segmentation of vessel structure in the retinal images without any user involvement. The method also handles complex structures such as sharp curved and branched vessels with varying lengths on images with a broad range of quality.

2. Description of proposed segmentation methods

The proposed retinal vessel segmentation method takes advantages of the rule-based unsupervised and supervised methods. The circular segmentation method uses neighboring pixels around the current pixel that is being processed to extract spatial consistency available in the image. For circular segmentation, color retinal images are transformed into grayscale images and then inverse images of the grayscale images are generated. Then a simple approach with circular sampling is employed in segmentation of the retinal vessels. On the other hand, the naive Bayes method as a supervised technique exploits a very small set of features to segment retinal vessels in retinal images. Finally, the proposed hybrid method combines the results generated by circular and Bayesian segmentation to achieve a better segmentation performance.

Basic steps in the proposed automatic retinal vessel segmentation and measurement system are classified into three groups. Steps in the first group are (1) generating a monochrome image and taking its inverse form, (2) applying the circular segmentation method, and (3) eliminating the mis-segmented fragments to obtain final circular segmentation results. Following steps in the second group are (4) collecting features from the color input image and (5) applying the Bayesian segmentation method. The last steps classified in the final group are (6) applying the hybrid segmentation approach and (7) evaluating segmentation results. A block diagram of the system is given in Figure 1.

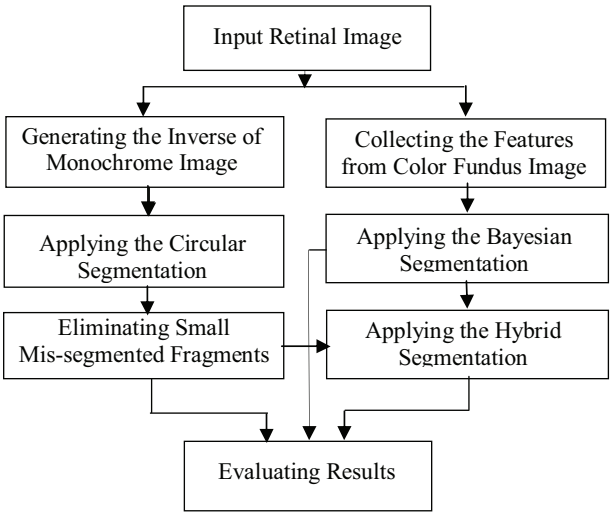

Figure 1. Block diagram of the vessel segmentation and measurement system.

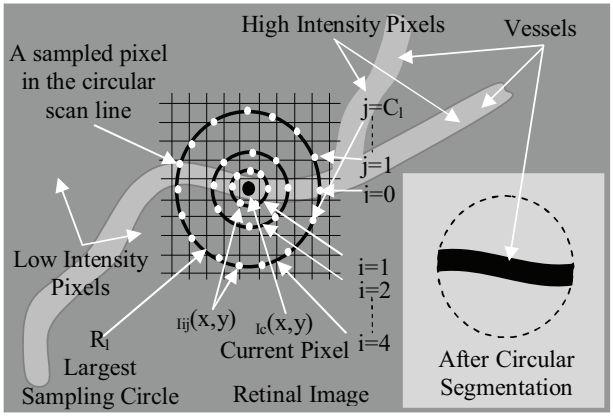

Figure 2. An illustration of circular sampling and segmentation of blood vessels.

2.1. Circular segmentation method

In segmentation, the circular sampling method is used for segmenting retinal vessels, as illustrated in Figure 2. Here, pixels around the currently processed pixel are sampled at a certain depth relative to the intensity value of the current pixel by using the circular sampling technique. The center of the sampling area is set as the current pixel. For example, if the current pixel's intensity is 150 and the threshold depth is set to 5, the threshold value for the current pixel is calculated to be 145 (150 – 5). Then the pixels in the circular scan lines around the current pixel are evaluated related to the current threshold value. The high-intensity pixels in the current circular sampling area are determined by using Eq. (1).

$$C_{i,j}(x,y) = \begin{cases} 1 & \text{if } I_{i,j}(x,y) > I_c(x,y) - D \\ 0 & \text{Otherwise} \end{cases} , \tag{1}$$

where $C_{i,j}(x,y)$, $I_{i,j}(x,y)$, $I_c(x,y)$, and D represent the high-intensity pixels in the current area, the intensity of pixels in circular scan lines in the current area, the intensity value of the current pixel, and the threshold depth, respectively. The threshold depth value is experimentally set to 4 for the pixels with standard deviations bigger than 0.1 and 3 for the other pixels, respectively.

As illustrated in the figure, the pixels around the current pixel or in the circular scan lines are sampled by using a circular sampling method, and then they are compared with the threshold value by using Eq. (1). The interval for the radius of the circles is experimentally calculated to be between 1 and 10 pixels. In other

words, the radius of the circles varies from 1 to 10 pixels to cover the vessels with the largest width. After the sampling process, the low- and high-intensity pixels shown as white and black areas are determined as part of the vessel and nonvessel areas, respectively. The total number of high-intensity pixels along the circular scan lines is calculated according to Eq. (2). The ratio of number of high-intensity pixels to total number of pixels is determined by using Eq. (3). If the rate of the high-intensity pixels ($R_t(x,y)$) is in the expected interval ($T_1 < R_t(x,y) < T_2$), the current pixel is set as a vessel; otherwise, the current pixel is set as a nonvessel. Finally, the yielding image is represented by $I_{CSI}(x,y)$ after circular segmentation. The threshold values (T_1 and T_2) are experientially set to 0.025 and 0.55, respectively. These threshold values are set to the fixed values to achieve the best segmentation performance. An original retinal image and its segmentation result are given in Figures 3a–3c.

$$T_{np}(x,y) = \sum_{i=1}^{R_l} \sum_{j=0}^{C_i} C_{ij}(x,y), \tag{2}$$

where $T_{np}(x,y)$, R_l, and C_i represent the total number of high-intensity pixels around the current pixel in the circular sampling area, the largest sampling circle's diameter, and the number of sampled pixels in the scan line of the sampling circle with diameter i as illustrated in Figure 2.

$$R_t(x,y) = T_{np}(x,y)/T_p, \tag{3}$$

where $R_t(x,y)$ is the rate of the number of high-intensity pixels to the total number of processed pixels in the current circular sampling area (T_p). Simply, the circular segmentation method consists of two stages, which are called circular segmentation and fragment elimination phases. In the application, a look-up table for circular sampling is determined only once and then the look-up table is used in classification of all of the pixels in the image in the circular segmentation.

Table 1. An example look-up table.

Indices	1	3	4	4	5	6	7	8
i	2	2	0	–2	–2	–2	0	2
j	0	2	2	2	0	–2	–2	–2

An example look-up table for the small sampling circle in Figure 2 is given in Table 1 for the current pixel $\{I_c(x,y)\}$.

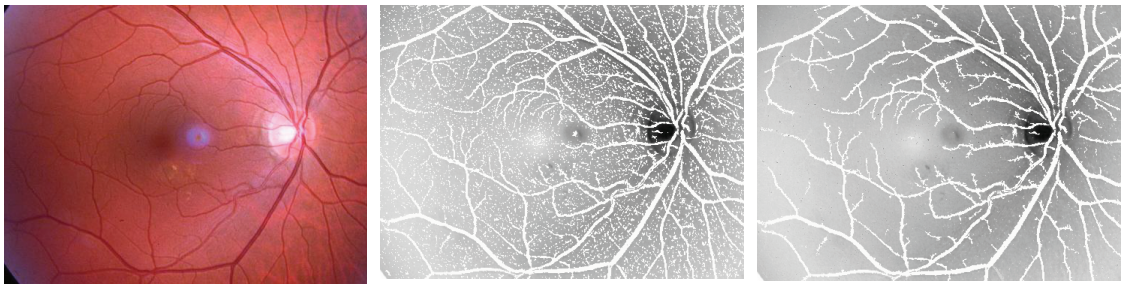

Figure 3. Original image (a); circular segmentation result before elimination of the fragment (b) and after the elimination of the nonvessel fragments (c).

2.1.1. Elimination of non-Vessel Fragments

The circular segmentation method produces small nonvessel fragments along with segmented vessel structures, as given in Figure 3b. These fragments should be removed from the final image to achieve a better segmentation result. An elimination method searches for small nonvessel areas such as square fragments. Therefore, the geometric form of fragments is used as an elimination criterion. Unfortunately, vessel structures are mostly in irregular geometric structures, which cause difficulties in differentiation of vessels from other structures. A practical approach is presented to estimate the fragment type, and to make some quantitative assessments of the fragments based on their shapes. Two methods are employed to estimate the shape and quantification of the fragments in the retinal images. First, a seed fill algorithm is used to measure the size and dimension of grains [30]. Here, each fragment in the image is filled by using seed fill algorithm, and then the areas of fragments are measured in pixels based on the number of pixel filled in each fragment.

By using the results of the seed fill algorithm, the maximum and minimum coordinates values along the x and y axes are calculated to decide whether the fragment is in a square-like structure or not. Consequently, the seed-filled fragment is checked to see whether it is in a thin-long fragment-like vessel structure or not by using Eq. (4). If the size of the fragment (SoF) is smaller than 14 pixels or the ratio (R_s) is bigger than 0.22, the fragment can be classified as a nonvessel-like structure and therefore eliminated excluding close fragments forming a line. Otherwise, the fragment is not eliminated. Here, the fragment is eliminated for larger values of the ratio, which is close to 1, since it does not depict a vessel-like structure. After elimination of the fragments, the segmentation result is shown in Figure 3c. The circular segmentation result is represented by $I_{CS}(x, y)$ after the fragment elimination process. In addition to this, some pixels with unexpected colors and intensity values such as bright lesions are also eliminated by using the Bayesian classifier given in the next section.

$$R_s = 100 * SoF/(1 + Mw * Mw), \tag{4}$$

where R_s, SoF, and Mw stand for the similarity rate, size of fragment in number of pixels, and maximum width of the fragment along the x or y axis, respectively. The similarity rate is the measure of how similar a fragment is to a square geometric form. If the similarity value is close to 0, the fragment is depicted as a vessel-like structure. Conversely, if the value is greater than 22, the fragment is depicted as a square-like structure. The maximum width (Mw) is set to the maximum width of the fragment along the x or y axis.

2.2. Bayesian segmentation method

In this section, the naive Bayes method as a supervised approach is introduced for segmentation of the retinal vessels. The naive Bayes classifier, introduced in this paper, uses a very small set of features to segment the retinal vessels efficiently. These features are colors (R, G, B) and intensity values; color ratios of pixels such as $G/(R + G), B/(R + B)$, and $B/(G + B)$; and R_t and R_s values. The proposed Bayesian classification approach uses only nine features to segment retinal vessels efficiently [31]. The mean, standard deviation (SD), and P-values of the features used in this application are given in Table 2 for vessel and nonvessel areas. In segmentation, the classifier given in Eq. (5) is used to extract vessel structures in retinal fundus images. In the application, an independent probability distribution is determined for each of these features and then pixels are classified by employing the equation. Here, the Bayesian segmentation method is applied in two stages, which are training and classification. After the training, the classifier is applied to each pixel of the input image to

generate the Bayesian segmentation result ($I_{BS}(x,y)$).

$$\text{Classify } (f_1,...,f_n) = \max_k \left\{ p(C_k) \prod_{i=1}^{n} p(f_i|C_k) \right\}, \tag{5}$$

where C, n, k, f, and i stand for classes, number of features, class variables, features, and feature indices, respectively. $p(f_i|C_k)$ and $p(C_k)$ represent the independent probability distributions and class priority, respectively [32].

Table 2. The mean, SD, and P-values of the features used in the application.

Features	Vessel			Nonvessel		
	Mean	SD	P-value	Mean	SD	P-value
Red (R)	183.49	19.37	0.5150	196.10	11.85	0.2873
Green (G)	82.35	15.38	0.1547	104,24	9.61	0.0228
Blue (B)	45.37	5.55	0.0308	57.37	4.34	0.0058
Intensity	108.77	12.03	0.1052	128.76	7.28	0.0061
$G/(R+G)\times$ *100*	35.53	8.01	0.2543	44.67	5,57	0.1031
$B/(R+B)\times$ *100*	18.81	4.634	0.2597	24.03	3.75	0.1645
$B/(G+B)\times$ *100*	38.85	5.75	0.2526	32.27	3.34	0.488
$R_t\times$ *100*	48.51	11.59	0.0004	71.25	17,80	0.0209
R_s	17.83	4.49	0.0257	27.76	6.78	0.1397

The proposed method uses a very small set of features to train the naive Bayes classifier under Gaussian distribution and to segment retinal vessels. For each feature, a probability and probability distribution are computed from the training set for the vessels and other areas in the images. For each class, the probability distributions of features are calculated, and then the class probability and the probabilities of features for each class are multiplied to classify the pixel with maximum value. Results show that the proposed Bayesian classifier quite successfully segments the vessels in retinal fundus images.

2.2.1. Selective sampling

In the training of the naive Bayes classifier, choosing correct training samples is important to perform an efficient segmentation process. In most of the applications, manual segmentation results are used to select training samples. Here, manual over- and undersegmentation, especially in the case of narrow and small vessels, causes wrong training samples to be chosen. In this application, training samples are selected by just clicking on the image as given in Figure 4. In addition to this, a selective sampling technique is employed to choose correct training samples. Thus, the selective sampling technique eliminates the false samples that are not representing its class based on the intensity and color values of the sample that should be in an expected interval. For example, the value of feature R_t should be in between 0.025 and 0.55. Hence, false samples are eliminated from the training samples by using the selective sampling method. As a result, the naive Bayes classifier is trained using only correct samples to achieve a better segmentation. In addition, the training process of the naive Bayes classifier is also reduced to a few minutes by using the selective sampling technique. For further improvement, the user may also click on more (good) samples if necessary. This reshapes the independent probability distribution positively. An experimental result of the selective sampling method is given in Figure 4.

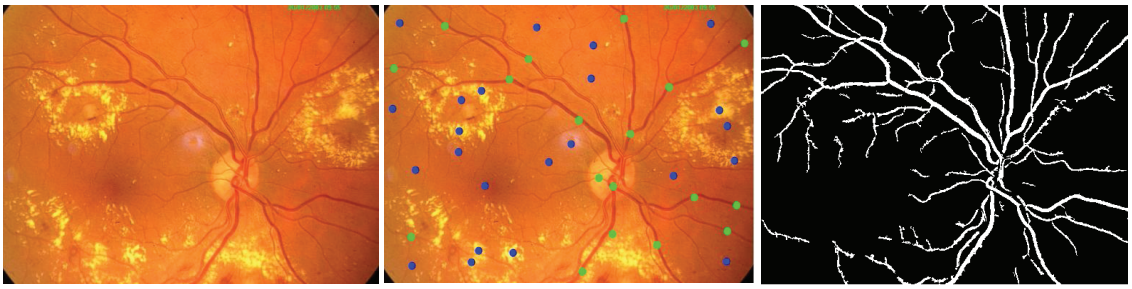

Figure 4. Original image (a), sampling points on the original image (b), and segmentation results (c).

2.3. Hybrid segmentation method

The hybrid segmentation method combines circular and Bayesian segmentation results to achieve a better segmentation. As shown in Figure 5, the overlapping pixels of circular and Bayesian segmentation are counted as true segmented pixels. If a pixel is segmented as a vessel by both methods, the segmentation result for the pixel is set as positive. On the contrary, if a pixel is segmented as a nonvessel by both methods, the segmentation decision for the pixel is set as negative. On the other hand, if the segmentation results of circular and Bayes segmentations are not the same for a pixel, the pixel is evaluated according to its distances from positive and negative segmented areas according to Eq. (6).

$$S_r = d_1/(d_1 + d_2), \tag{6}$$

where S_r represents the segmentation results for nonoverlapping segmentations, and d_1 and d_2 stand for the distances as illustrated in Figure 5.

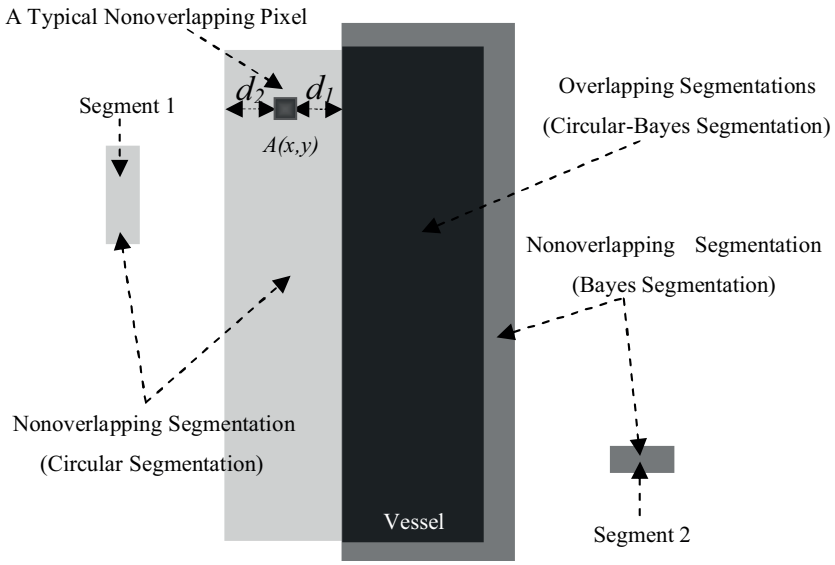

Figure 5. An illustration of the hybrid segmentation method.

A simple illustration of hybrid segmentation is given in Figure 5. As given in the illustrations, nonoverlapping segmentation results are evaluated according to the distances from the positive and negative segmented areas. As illustrated in the figure, d_1 and d_2 are the shortest distances from pixel $A(x, y)$ to positive and

negative segmented areas, respectively. Hence, the nonoverlapping segmentation results are evaluated by using Eq. (6). The minimum values of d_1 and d_2 are set to 1. Some pixels segmented as positive that have no connection or that are more than three pixels away from the overlapping area, such as segment 1 and segment 2, are eliminated. To improve the quality of the segmentation results, a low-pass filtering (averaging) for preprocessing and a simple filing technique for postprocessing are performed. The filing technique checks the neighboring pixels classified as nonvessel structures. If a nonvessel pixel has at least four neighboring pixels segmented as vessel, it is also set as vessel by applying the postprocessing.

3. Evaluating the segmentation results

Two data sets are used for training and evaluation of the system. The DRIVE [19] and STARE [22] data sets that include 60 manually labeled images are used in tests. The DRIVE database consists of forty images with 768 $\times$ 584 pixels of resolution (10 for training and 10 for testing), and manually segmented forms of those images. The masks of the images were also provided for the field of view. The images were manually segmented by three ophthalmologists, two of whom segmented the test images while the other person segmented the training set. The manually segmented test set is separated into two groups, which are set A and B. Performance of the proposed system is examined on the test sets by using set A, which is employed as ground truth data. For performance comparison, images in set B were tested against the images in set A. Apart from the DRIVE database, the STARE database includes 20 retinal images with resolution of 700 $\times$ 605 pixels. All images were manually segmented by two graders. The first grader's segmentations are chosen as ground truth data, on which the performance of the proposed system was measured. The other images presented in the paper were taken from a digital fundus camera at the Department of Ophthalmology, Faculty of Medicine, Karadeniz Technical University.

In this study, the performance of the segmentation methods are compared based on measurement tests. The methods measure overlapping and nonoverlapping segmentation results to determine the accuracy of segmentation results. Proposed algorithms were evaluated in terms of true positive rate, false positive rate, sensitivity, specificity, and accuracy. In most of the studies, these measurements are used to quantify segmentation results of retinal vessels. Accuracy of the segmentation result of retinal images is measured by using Eq. (7).

$$\{\mathrm{Acc}\} = (\mathrm{TS} + \mathrm{TN})/(\mathrm{TS} + \mathrm{TN} + \mathrm{FP} + \mathrm{FN}), \tag{7}$$

where $\{Acc\}$, TS, TN, FP, and FN represent the accuracy of segmentation results and true segmented, true negative segmented, oversegmented, and undersegmented pixels, respectively. Here, true segmented pixels are the overlapping pixels with the manually segmented ones and the true negative segmented pixels represent the inverse of manually segmented pixels. In this experiments, 10-fold cross-validation is also used, as commonly adopted in the literature.

4. Results

In this paper, a simple and fast hybrid method is proposed for extracting and measuring the vessel structures in retinal fundus images. This method utilizes circular and Bayesian approaches to segment vessel structures in fundus images efficiently. Experiments and measurements were performed on a PC with Intel Core 2 Quad-2.50 GHz CPU and 4.00 GB RAM. The threshold applied in the segmentation is established based on experiments by using the training data set. Proposed experiments prove that the proposed automatic vessel segmentation

methods work fine and the system needs little adjustment to set the threshold values; it is also easily trained to achieve an efficient segmentation process.

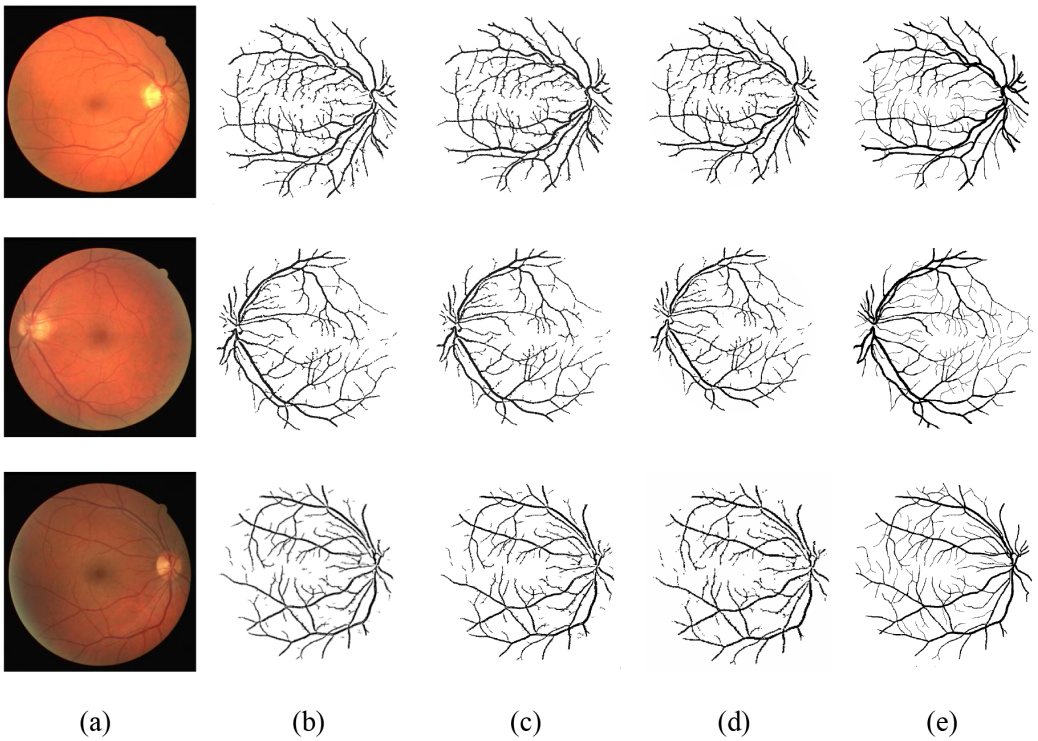

Figure 6. Original retinal image (a); circular (b), Bayesian (c), and hybrid segmentation results (d); and manual segmentation of the images from set A taken from the DRIVE data set (e).

Figure 6 presents some segmentation results generated by using circular, Bayesian, and hybrid segmentation approaches on images obtained from the DRIVE database. In the figure, along with the original image, its segmented forms by circular, Bayesian, and hybrid approaches are given, as well as manual segmentation results. Segmentation accuracies of the images at first, second, and third lines for hybrid approach are 0.962, 0.964, and 0.963, respectively.

Figure 7 presents some segmentation results generated by using the circular, Bayesian, and hybrid segmentation approaches on images obtained from the STARE database. In the figure, the original images; their segmented forms by circular, Bayesian, and hybrid segmentation approaches; and their manually segmented forms are presented. Segmentation accuracies of the images at first, second, and third lines for the hybrid approach are 0.959, 0.957, and 0.965, respectively. The middle image includes some degeneration or pathological cases.

Segmentation performances of proposed methods were compared with some previously developed vessel segmentation methods. The ROC curves, generated for images obtained from DRIVE and STARE databases using the proposed hybrid segmentation, ridge-based vessel segmentation [23], two-dimensional Gabor wavelet and supervised classification [24], two-dimensional matched filter methods [29], and human observations, are shown in Figures 8 and 9. These figures present the ROC curves for varying thresholds. The manual segmentation results of set B and the second grader's results are shown as marked points in the corresponding images. In this application, true and false positive fractions are calculated over all test images.

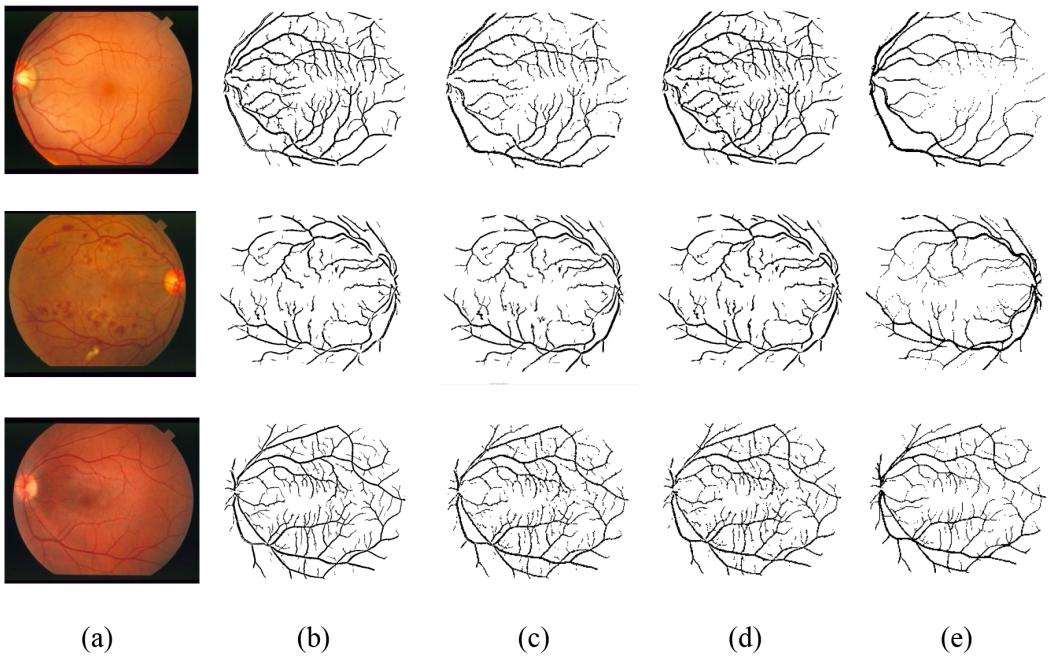

Figure 7. Original retinal image (a); circular (b), Bayesian (c), and hybrid segmentation results (d); and manually segmented forms of images from first observer's data set obtained from STARE database (e).

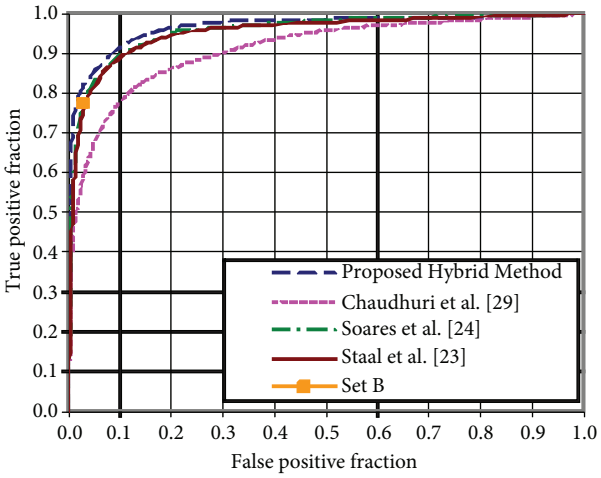

Figure 8. A comparison of performances of the segmentation methods applied to images from the DRIVE database.

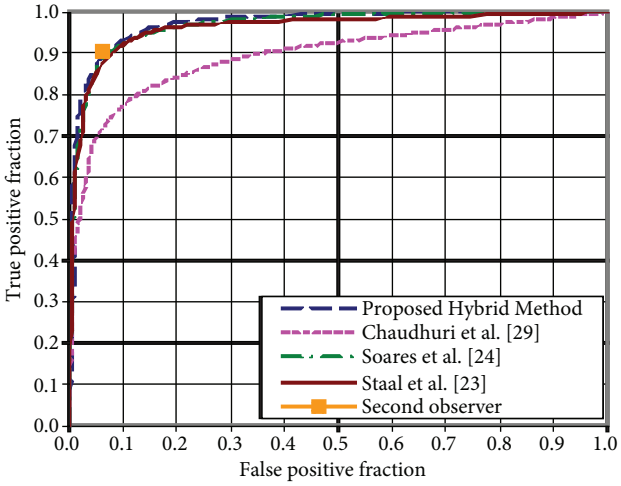

Figure 9. A comparison of performances of the segmentation methods on the STARE database.

The proposed methods for the automatic segmentation of the retinal vasculature in retinal images were examined on the images obtained from the DRIVE and STARE databases. Comparison of the proposed method and the other methods given in Table 3 presents the average accuracy of the proposed method for the test sets of the DRIVE and STARE databases. Two results are given in the table as R1 and R2. The first accuracy result in the table (R1) shows the performance of the proposed method against the first grader's manual segmentations. The second accuracy result (R2) is obtained considering the manual segmentations of both graders.

Table 3. Performances of vessel segmentation methods on DRIVE and STARE data sets.

Methods	Average accuracy		
	Data sets		General average
	DRIVE	STARE	
Circular segmentation	0.9461	0.9440	0.9451
Bayesian segmentation	0.9453	0.9441	0.9446
Hybrid (R1)	0.9550	0.9542	0.9549
Hybrid (R2)	0.9634	0.9576	0.9605
Chaudhuri et al. [29]	0.8773	-	0.8773
Hoover et al. [22]	-	0.9267	0.9267
Jiang et al. [27]	0.8911	0.9001	0.8956
Marín et al. [25]	0.9452	0.9526	0.9589
Mendonça et al. [9]	0.9452	0.9440	0.9446
Niemeijer [19]	0.9417	-	0.9417
Ricci et al. [13]	0.9563	0.9584	0.9573
Soares et al. [24]	0.9466	0.9480	0.9473
Staal et al. [23]	0.9441	0.9516	0.9479
You et al. [26]	0.9434	0.9497	0.9466
Zhang et al. [11]	0.9640	0.9087	0.9364
Second human observer	0.9473	0.9354	0.9414

Segmentation performances of proposed methods (circular, Bayesian, hybrid-(R1) and hybrid-(R2) segmentations) are given in the first four rows of the table. These results show that the proposed method is one of most efficient methods among the unsupervised and supervised methods. The average accuracy reported for some other methods, especially for supervised methods, are relatively higher, but those methods are more complex and costly in terms of computational complexity. They also require sensitive and difficult adjustments, and training to achieve the best performance. In terms of general average accuracy on both data sets, the proposed hybrid approach shows the best performance among all unsupervised and supervised methods as given in the table.

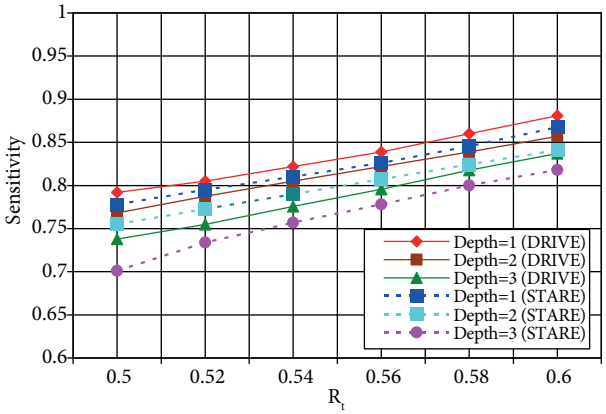

Figure 10. Sensitivity results of the proposed method for the threshold depths and various R_t values.

According to our experiments, automatic processing of an image takes less than 1 s, which takes up to 1 h in the case of manual segmentation. The proposed method shows a quite consistent and effective performance for the images with some degeneration or pathologies. The proposed methods are not complex or expensive and

they do not require very sensitive or difficult adjustments. The proposed methods can also easily be trained to achieve the best performance. Sensitivity and specificity values of the hybrid method for the DRIVE and STARE data sets are 0.782 and 0.977, and 0.758 and 0.978, respectively. To present the performance of the method, sensitivity results for the DRIVE and STARE data sets for various threshold depths and various R_t values are presented in the Figure 10. These results show that the threshold depth and R_t value may be chosen by the user for a better sensitivity value if necessary.

5. Conclusion and future work

The proposed segmentation approaches are the simplest, fastest, and most efficient methods among the unsupervised and supervised segmentation methods. Using the proposed methods, the complete segmentation of vessel structure in a retinal image can be performed in less than 1 s without any user involvement. As the results show, a large number of retinal fundus images with varying qualities are successfully segmented by the proposed techniques.

Previous segmentation methods are more complex, and they require more computational effort than the proposed methods because the proposed methods use only a few easily tunable threshold values. They can easily be trained for efficient segmentation of varying quality of retinal images. Other existing methods show various performances in detection and segmentation of blood vessels. These methods show over 90% detection and segmentation accuracy [9,11,23–24,29]. The segmentation accuracies of the proposed hybrid methods are about 95% on the same data sets.

The methods proposed for segmentation of retinal vessel structures in retinal images may also be used to segment other kinds of blood vessels in the detection of other diseases such as cardiovascular disease, which could be undertaken as future work. The test results also show that thin vessel structures cannot be fully detected in some cases. To improve the performance of the proposed methods, more efficient preprocessing and postprocessing operations may also be applied. Therefore, more efficient vessel segmentation techniques may be developed for further improvement.

Acknowledgments

The author would like thank A Hoover and JJ Staal and colleagues for making their databases publicly available. The author also thanks a faculty member of the Medical School at Karadeniz Technical University for providing the digital color fundus images used in the study.

References

[1] Köse C, İkibaş C. A personal identification system using retinal vasculature in retinal fundus images. Expert Syst Appl 2011; 38: 13670–13681.

[2] Lowell JA, Hunter A, Steel D, Basu A, Ryder R, Kennedy RL. Measurement of retinal vessel widths from fundus images based on 2-D modeling. IEEE T Med Imaging 2004; 23: 1196–1204.

[3] Köse C, Şevik U, İkibaş C, Erdöl H. Simple methods for segmentation and measurement of diabetic retinopathy lesions in retinal fundus images. Comput Meth Prog Bio 2011; 107: 274–293.

[4] Gang L, Chutatape O, Krishnan SM. Detection and measurement of retinal vessels in fundus images using amplitude modified second-order Gaussian filter. IEEE T Bio-Med Eng 2002; 49: 168–172.

[5] Kayıkçıoğlu T, Gangal A, Turhal M, Köse C. A surface-based method for detection of coronary vessel boundaries in poor quality X-ray angiogram images. Pattern Recogn Lett 2002; 23: 783–802.

[6] Yavuz Z, İkibaş C, Köse C. A simple analytic approach for tracking retinal vessel and measuring their diameters. In: International Conference on Bioinformatics; 20–23 January 2010; Valencia, Spain.

[7] Cosatto VF, Liew G, Rochtchina E, Wainwright A, Zhang Y, Hsu W, Lee ML, Lau QP, Hamzah HH, Mitchell P et al. Retinal vascular fractal dimension measurement and its influence from imaging variation: results of two segmentation methods. Curr Eye Res 2010; 35: 850–856.

[8] Zhou H, Schaefer G, Liu T, Lin F. Segmentation of optic disc in retinal images using an improved gradient vector flow algorithm. Multimed Tools Appl 2010; 49: 447–462.

[9] Mendonça AM, Campilho A. Segmentation of retinal blood vessels by combining the detection of centerlines and morphological reconstruction. IEEE T Med Imaging 2006; 25: 1200–1213.

[10] Marwan DS, Eswaran C, Mueen A. An automated blood vessel segmentation algorithm using histogram equalization and automatic threshold selection. J Digit Imaging 2011; 24: 564–572.

[11] Zhang Y, Hsu W, Lee ML. Segmentation of retinal vessels using nonlinear projections. In: IEEE International Conference on Image Processing; 16–19 September 2007; San Antonio, TX, USA. New York, NY, USA: IEEE. pp. 541–544.

[12] Bhuiyan A, Nath B, Chua J, Kotagiri R. Blood vessel segmentation from color retinal images using unsupervised texture classification. In: IEEE International Conference on Image Processing; 16–19 September 2007; San Antonio, TX, USA. New York, NY, USA: IEEE. pp. 521–524.

[13] Ricci E, Perfetti R. Retinal blood vessel segmentation using line operators and support vector classification. IEEE T Med Imaging 2007; 26: 1357–1365.

[14] Vermeer KA, Vos FM, Lemij HG, Vossepoel AM. A model based method for retinal blood vessel detection. Comput Biol Med 2004; 34: 209–219.

[15] Ghaderi R, Hassanpour H, Shahiri M. Retinal vessel segmentation using the 2-D Morlet wavelet and neural network. In: International Conference on Intelligent and Advanced Systems; 25–28 November 2007; Kuala Lumpur, Malaysia. New York, NY, USA: IEEE. pp. 1251–1255.

[16] Perfetti R, Ricci E, Casali D, Costantini G. Cellular neural networks with virtual template expansion for retinal vessel segmentation. IEEE T Circuits-II 2007; 54: 141–145.

[17] Chutatape O, Zheng L, Krishman S. Retinal blood vessel detection and tracking by matched Gaussian and Kalman filters. In: Proceedings of the 20th Annual International Conference of the IEEE Engineering in Medicine and Biology Society; 1998; Hong Kong. New York, NY, USA: IEEE. pp. 3144–3149.

[18] Marín D, Aquino A, Gegúndez-Arias ME, Bravo JM. A new supervised method for blood vessel segmentation in retinal images by using gray-level and moment invariants-based features. IEEE T Med Imaging 2011; 30: 146–158.

[19] Niemeijer M, Staal J, van Ginneken B, Loog M, Abràmoff MD. Comparative study of retinal vessel segmentation methods on a new publicly available database. SPIE Med Imag 2004; 5370: 648–656.

[20] Köse C, İkibaş C. Segmentation of coronary vessel structures in X-ray angiogram images by using spatial pattern matching method. In: 23rd International Symposium on Computer and Information Sciences; 27–29 October 2009; İstanbul, Turkey. New York, NY, USA: IEEE. pp. 1–6.

[21] Zana F, Klein JC. Segmentation of vessel-like patterns using mathematical morphology and curvature evaluation. IEEE T Image Process 2001; 10: 1010–1019.

[22] Hoover A, Kouznetsova V, Goldbaum M. Locating blood vessels in retinal images by piecewise threshold probing of a matched filter response. IEEE T Med Imaging 2000; 19: 203–210.

[23] Staal J, Abramoff MD, Niemeijer M, Viergever MA, Ginneken BV. Ridge-based vessel segmentation in color images of the retina. IEEE T Med Imaging 2004; 23: 501–509.

[24] Soares JVB, Leandro JJG, Cesar RM Jr, Jelinek HF, Cree MJ. Retinal vessel segmentation using the 2-D Gabor wavelet and supervised classification. IEEE T Med Imaging 2006; 25: 1214–1222.

[25] Marín D, Aquino A, Gegúndez-Arias ME, Bravo JM. A new supervised method for blood vessel segmentation in retinal images by using gray-level and moment invariants-based features. IEEE T Med Imaging 2011; 30: 146–158.

[26] You X, Peng Q, Yuan Y, Cheung Y, Lei J. Segmentation of retinal blood vessels using the radial projection and semi-supervised approach. Pattern Recogn 2011; 44: 2314–2324.

[27] Jiang X, Mojon D. Adaptive local thresholding by verification-based multithreshold probing with application to vessel detection in retinal images. IEEE T Pattern Anal 2003; 25: 131–137.

[28] Lam BSY, Yan H. A novel vessel segmentation algorithm for pathological retina images based on the divergence of vector fields. IEEE T Med Imaging 2008; 27: 237–246.

[29] Chaudhuri S, Chatterjee S, Katz N, Nelson M, Goldbaum M. Detection of blood vessels in retinal images using two-dimensional matched filters. IEEE T Med Imaging 1989; 8: 263–269.

[30] Rogers DF. Procedural Elements for Computer Graphics. New York, NY, USA: McGraw-Hill, 1988.

[31] Duda RO, Hart PE, Stork DG. Pattern Classification. Chichester, UK: John Wiley & Sons, 2001.

[32] Peng F, Schuurmans D. Combining naive Bayes and n-gram language models for text classification. Lect Notes Comp Sci 2003; 2633: 335–350.